Systems/Circuits

Contralateral Afferent Input to Lumbar Lamina I Neurons as a Neural Substrate for Mirror-Image Pain

Liliana L. Luz,[1,2] Susana Lima,[1,2] Elisabete C. Fernandes,[1,2] Eva Kokai,[3] Lidia Gomori,[3] Peter Szucs,[3,4] and Boris V. Safronov[1,2]

[1]Instituto de Investigação e Inovação em Saúde, Universidade do Porto, Porto 4200-135, Portugal, [2]Neuronal Networks Group, Instituto de Biologia Molecular e Celular (IBMC), Universidade do Porto, Porto 4200-135, Portugal, [3]Department of Anatomy, Histology and Embryology, Faculty of Medicine, University of Debrecen, Debrecen H-4032, Hungary, and [4]ELKH-DE Neuroscience Research Group, Debrecen H-4032, Hungary

Mirror-image pain arises from pathologic alterations in the nociceptive processing network that controls functional lateralization of the primary afferent input. Although a number of clinical syndromes related to dysfunction of the lumbar afferent system are associated with the mirror-image pain, its morphophysiological substrate and mechanism of induction remain poorly understood. Therefore, we used *ex vivo* spinal cord preparation of young rats of both sexes to study organization and processing of the contralateral afferent input to the neurons in the major spinal nociceptive projection area Lamina I. We show that decussating primary afferent branches reach contralateral Lamina I, where 27% of neurons, including projection neurons, receive monosynaptic and/or polysynaptic excitatory drive from the contralateral Aδ-fibers and C-fibers. All these neurons also received ipsilateral input, implying their involvement in the bilateral information processing. Our data further show that the contralateral Aδ-fiber and C-fiber input is under diverse forms of inhibitory control. Attenuation of the afferent-driven presynaptic inhibition and/or disinhibition of the dorsal horn network increased the contralateral excitatory drive to Lamina I neurons and its ability to evoke action potentials. Furthermore, the contralateral A$\beta\delta$-fibers presynaptically control ipsilateral C-fiber input to Lamina I neurons. Thus, these results show that some lumbar Lamina I neurons are wired to the contralateral afferent system whose input, under normal conditions, is subject to inhibitory control. A pathologic disinhibition of the decussating pathways can open a gate controlling contralateral information flow to the nociceptive projection neurons and, thus, contribute to induction of hypersensitivity and mirror-image pain.

Key words: **dorsal horn; dorsal root potentials; marginal zone; nociception; presynaptic inhibition; primary afferents**

Significance Statement

We show that contralateral Aδ-afferents and C-afferents supply lumbar Lamina I neurons. The contralateral input is under diverse forms of inhibitory control and itself controls the ipsilateral input. Disinhibition of decussating pathways increases nociceptive drive to Lamina I neurons and may cause induction of contralateral hypersensitivity and mirror-image pain.

Introduction

Mirror-image pain, a pain perceived as arising from the body region contralateral to the actual injury site, is associated with many clinical syndromes (Huang and Yu, 2010; Konopka et al., 2012). It is characterized by allodynia and hyperalgesia which were described both in humans and rodent models of thermal injury, neuropathy and inflammation (Coderre and Melzack, 1991; Coderre et al., 1993; Huang and Yu, 2010; Konopka et al., 2012). Mirror-image pain is assumed to be caused by pathologic alterations of signaling pathways, e.g., glial or neurochemical, that link the two sides of the body (Coderre et al., 1993; Koltzenburg et al., 1999; Milligan et al., 2003; Huang and Yu, 2010; Cheng et al., 2014). However, the complex nature of this mysterious phenomenon is still poorly understood because of insufficient knowledge on organization of its neural substrate and mechanisms of induction.

At the spinal cord level, morphophysiological basis of mirror-image pain is provided by bilateral organization of the sensory processing network that comprises decussating primary afferent fibers (Culberson et al., 1979; Light and Perl, 1979a; Marfurt and

Received Oct. 6, 2022; revised Feb. 17, 2023; accepted Mar. 9, 2023.

Author contributions: L.L.L. and B.V.S. designed research; L.L.L., S.L., E.C.F., E.K., L.G., and P.S. performed research; L.L.L. and P.S. analyzed data; B.V.S. wrote the paper.

This work was funded by National Funds through FCT - Fundação para a Ciência e a Tecnologia, I.P., under the project UIDB/04293/2020 and supported by FEDER - Fundo Europeu de Desenvolvimento Regional funds through the COMPETE 2020-Operacional Program for Competitiveness and Internationalization (POCI), Portugal 2020, and by Portuguese funds through FCT-Fundacão para a Ciência e a Tecnologia/Ministério da Ciência, Tecnologia e Ensino Superior in the framework of the Project PTDC/NEU-NMC/1259/2014 (POCI-01-0145-FEDER-016588). E.C.F. and L.L.L. were supported by FCT Fellowships SFRH/BD/118129/2016 and SFRH/BPD/120097/2016, respectively. P.S., E.K., and L.G. were supported by Hungarian Brain Research Program Grants KTIA_NAP_13-2-2014-0005 and 2017-1.2.1-NKP-2017-00002.

The authors declare no competing financial interests.

Correspondence should be addressed to Boris V. Safronov at safronov@ibmc.up.pt.

https://doi.org/10.1523/JNEUROSCI.1897-22.2023

Rajchert, 1991), commissural dorsal horn interneurons (Petkó and Antal, 2000; Petkó et al., 2004), bilaterally projecting spinothalamic and spinoparabrachial neurons (Burstein et al., 1990; Spike et al., 2003) as well as a population of Lamina I neurons projecting via the ipsilateral anterolateral tract (Antal et al., 2016). The decussating nociceptive afferents are numerous in the medullary, cervical, thoracic and sacral cord (Culberson et al., 1979; Light and Perl, 1979a; Marfurt and Rajchert, 1991), that can explain a high occurrence rate of the mirror-image pain related to the structures innervated by these afferents (Khan et al., 2007; Mathew et al., 2008). The decussating thin afferent fibers are much less frequent in the lumbar segments of the spinal cord (Culberson et al., 1979; Light and Perl, 1979a; Shehab and Hughes, 2011), and it is not clear whether they provide a functional excitatory synaptic drive to the contralateral nociceptive processing neurons. In the lumbar cord, the contralateral afferent inputs, both excitatory and inhibitory, were recorded in dorsal horn neurons (Fitzgerald, 1982, 1983). However, little is known about the contralateral afferent supply of neurons in the major spinal nociceptive projection area Lamina I. Such knowledge could be relevant for understanding mechanisms of mirror-image pain related to pathology of the lumbar afferent system (Coderre and Melzack, 1991; Milligan et al., 2003; Konopka et al., 2012; Cheng et al., 2014; Su et al., 2018).

Besides, we have recently shown that the C-fiber input to Lamina I is subject to presynaptic inhibition driven by the ipsilateral homosegmental and heterosegmental Aβ-afferents, Aδ-afferents, and C-afferents (Fernandes et al., 2020, 2022a). The presynaptic inhibition might also be driven by the contralateral afferent system, since earlier studies had shown that afferent stimulation induces contralateral dorsal root potential (DRP; Barron and Matthews, 1938; Lloyd and McIntyre, 1949; Wall and Lidierth, 1997) and contralateral inhibition of the C-fiber-evoked activity of deep dorsal horn neurons with duration similar to that of DRP (Mendell, 1966; Brown et al., 1973). Furthermore, it is also possible that, under normal conditions, the contralateral nociceptive fiber input to Lamina I is controlled by a feedforward inhibitory circuitry. This circuitry could prevent the neurons from receiving nociceptive input from the contralateral body regions, and its pathologic disinhibition can cause mirror-image pain.

Here, we aimed to study whether the contralateral afferents supply lumbar Lamina I neurons, and whether this supply is under inhibitory control and can affect the ipsilateral afferent input. We also asked whether disinhibition of the spinal network can increase contralateral synaptic drive to Lamina I.

Materials and Methods

Ethical approval

For primary afferent labeling, four-week-old Wistar rats of either sex were anaesthetized with isoflurane (Baxter) delivered by SomnoSuit low-flow system (Kent Scientific). The depth of narcosis was ascertained by the disappearance of nocifensive responses to pinching the tail or hind paw of the animal. This procedure was approved by the institution's animal welfare committee (8/2015/DEMÁB). For the whole-cell recording in the *ex vivo* spinal cord, Wistar rats (postnatal days, P13–P20) of both sexes were killed by decapitation in accordance with Portuguese national guidelines (Direcção Geral de Alimentação e Veterinária, Ministério da Agricultura) after intraperitoneal anesthesia with Na^+-pentobarbital (30 mg/kg) and subsequent monitoring for lack of pedal withdrawal reflexes. The experiments were conducted according to the guidelines laid down by the institution's animal welfare committee (Comissão de Ética do Instituto de Biologia Molecular e Celular).

Primary afferent labeling

The dorsal surface of the thigh of the anaesthetized animal was shaved and disinfected with Betadine. A 2-cm longitudinal (parallel with the femur) incision was made on the thigh at the level of the L5-to-L6 vertebra transition. The gluteus maximus and biceps femoris muscles were carefully separated to gain access to the sciatic nerve. The AAV-CAG-tdTomato viral vector (2 µl, AddGene, 59 462-AAVrg) was injected into the sciatic nerve using a 1.2-µl Hamilton syringe with a 26-G needle. After the injection, the skin was closed with coated VICRYL 5–0 absorbent suture (Ethicon). For the postoperative analgesia, a combination of intraperitoneal paracetamol (200 mg/kg) and locally applied bupivacaine was used. The animal was returned to its cage after awakening. After a survival period of one week, animals were deeply anaesthetized with intraperitoneal sodium pentobarbital (50 mg/kg) and transcardially perfused by 4% paraformaldehyde. The lumbar cord with the attached dorsal roots, dorsal root ganglia (DRGs) and spinal nerves was removed and fixed for at least 24 h at 4°C. The sciatic viral vector injections were done in four animals, three of which were used for the estimation of the number of labeled DRG neurons and one for the spinal cord immunocytochemistry.

Quantification of labeled DRG neurons

According to the earlier study (Swett et al., 1991), the sciatic nerve of young and middle age rats contains axons of ~10,000 primary afferent neurons. Their somata are located mostly in the L4 and L5 DRGs (98–99%) and, to much lesser degree, in the L3 (1.2%) and L6 (0.4%) DRGs. Therefore, we collected ipsilateral, to the side of injection, L3–L6 DRGs, embedded in agar (4–6%) and sectioned (100-µm thickness) parallel to the dorsal root using a tissue slicer (VT1000, Leica). Sections were washed with 0.1 M phosphate buffer. Neuronal somata and nuclei were stained with a fluorescent Nissl stain (NeuroTrace, Thermofisher Scientific) and DAPI (Sigma), respectively. Sections were mounted in Hydromount medium (National Diagnostics) and series of optical images were acquired at a 3.5-µm step using an Olympus FV3000 confocal system with a 10× objective. All L3–L6 ganglia were inspected and, in agreement with Swett and colleagues (Swett et al., 1991), the vast majority of labeled somata were found in the L4 and L5 DRGs (Fig. 1*A*). In three transfected animals, we counted a total of 22, 131, and 264 tdTomato-labeled DRG neurons (Fig. 1*B*). Thus, our approach sparsely labeled <3% of the sciatic afferents (Swett et al., 1991). Largest cross-sectional diameter of each labeled neuron was manually measured using FIJI software (Schindelin et al., 2012) and compared with those of four directly adjacent nonlabeled neighbors. The mean diameters of labeled neurons in the three animals were 31.3 ± 1.7 µm ($n = 22$), 26.4 ± 0.6 µm ($n = 131$), and 28.9 ± 0.6 µm ($n = 264$). The mean diameters of the nonlabeled control neuron population in the three animals were 32.2 ± 1.0 µm ($n = 88$), 31.1 ± 0.4 µm ($n = 524$), and 32.2 ± 0.3 µm ($n = 1056$). For animals 2 and 3, this difference was significant ($p < 0.001$), suggesting that the sciatic nerve transfection in our experiments resulted in labeling mostly sensory small and medium sized DRG neurons (Swett et al., 1991).

Immunocytochemistry and histochemistry

To reveal contralateral projections of primary afferents, lumbosacral L3-S1 segments of the spinal cord were dissected and postfixed for 3 h in 4% paraformaldehyde. The cord was serially sectioned (100-µm thickness) in the transverse plane using a tissue slicer (VT1000, Leica). After blocking (30 min) with bovine serum albumin (Sigma), the sections were incubated (2 d, 4°C) in a cocktail of primary antibodies containing mouse anti-synaptophysin (1:200, Sigma), rabbit anti-MAP (1:1000, Sigma) and biotynilated IB4 (1:500, Invitrogen). All antibodies were dissolved in a 0.1 M phosphate buffer supplemented with 0.3% Triton X-100 and bovine serum albumin. The sections were washed in phosphate buffer (3 × 10 min) following each incubation step except that with the blocking agent. Species-specific secondary antibodies were raised in donkey or goat and conjugated to fluorescent dyes CF405 (1:1000, Invitrogen) and CF647 (1:1000, Invitrogen). The biotinylated IB4 was revealed by Alexa 488-conjugated streptavidin (1:1000, Jackson ImmunoResearch) and neuronal somata

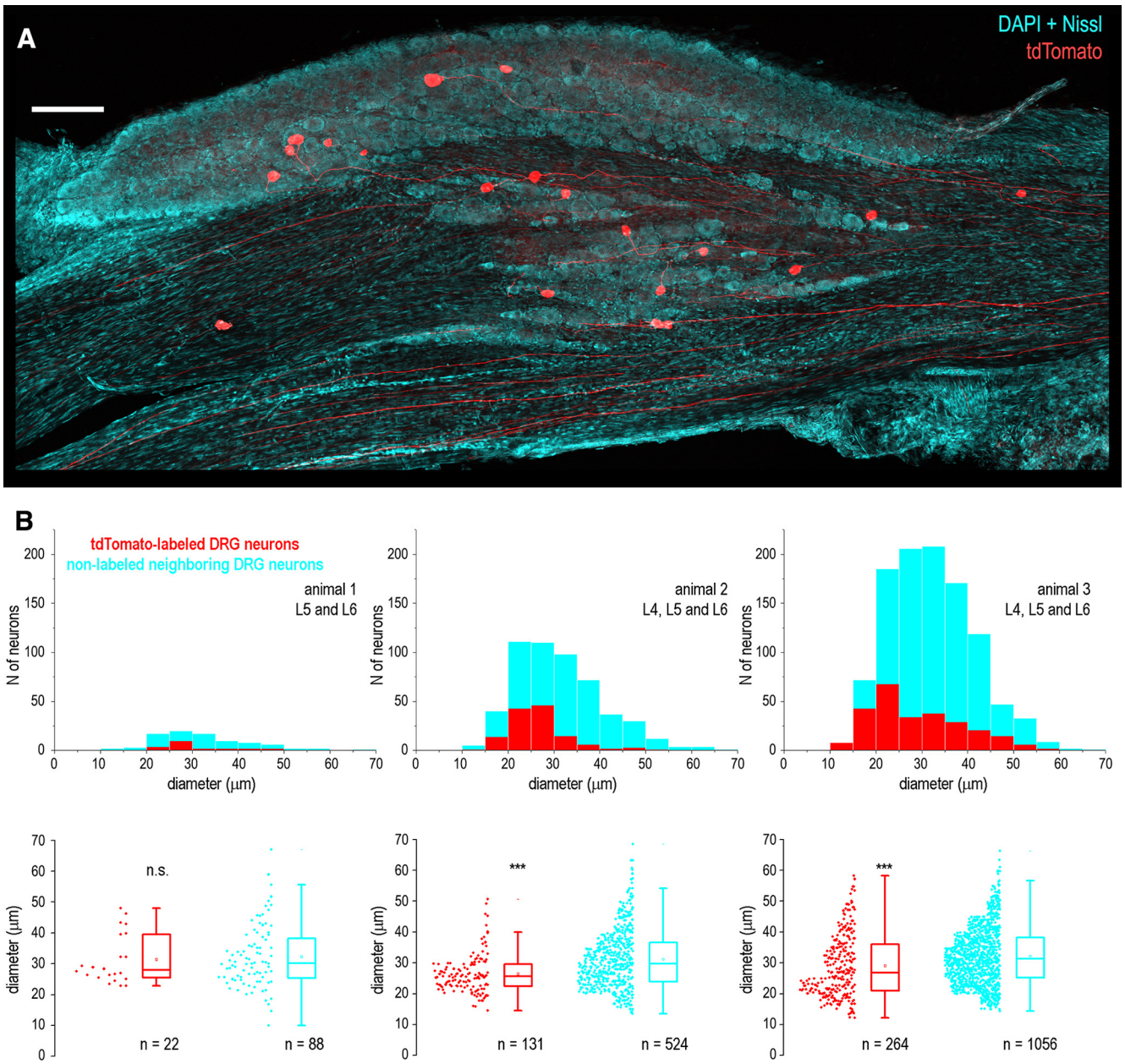

Figure 1. Labeling of primary sensory neurons after sciatic injection of AAV-CAG-tdTomato viral vector. ***A***, DRG neurons expressing tdTomato (red) after the sciatic injection of viral vector. A low-magnification montage of 3 image tiles showing a Z-projection of 22 optical planes from a 100-μm-thick section of the L5 DRG. DAPI and Nissl staining (both cyan) revealed nuclei and cytoplasm of all DRG neurons. Scale bar, 200 μm. ***B***, Distribution histograms of the largest cross-section diameters of all tdTomato-labeled and neighboring nonlabeled DRG neurons in three animals. Below, box-plots showing the largest cross-sectional diameter of all labeled and neighboring nonlabeled DRG neurons in the same three animals. The box indicates the 25th–75th percentile range, whiskers are set to outliers (coefficient, 1.5), square shows mean and the horizontal line indicates the median. n.s., not significant; ***$p < 0.001$.

were stained with a fluorescent Nissl stain (NeuroTrace, Thermofisher Scientific). Sections were mounted in Hydromount medium (National Diagnostics) and series of optical images at a 0.5-μm step were acquired using an Olympus FV3000 confocal system with a 10× or 40× oil-immersion objective.

To reveal biocytin after whole-cell recording, the tissue block with filled neurons was fixed in 4% paraformaldehyde at 4°C for at least 48 h. After embedding in agar, transverse serial sections of 100-μm thickness were cut with a tissue slicer (VT 1000S, Leica). The sections were permeabilized with 50% ethanol, treated according to the avidin–biotinylated horseradish peroxidase method (ExtrAvidin-Peroxidase, diluted 1:1000) followed by a diaminobenzidine chromogen reaction. Sections were counterstained with 1% toluidine blue, dehydrated and mounted with DPX (Fluka). Lamina I neurons were identified as projection neurons (PNs) or local-circuit neurons (LCNs) based on the structure of their axon (Szucs et al., 2010, 2013; Fernandes et al., 2016). The major axon of a PN crossed the spinal cord midline in the anterior commissure, whereas an axon of an LCN branched extensively within the ipsilateral dorsal horn and did not cross the spinal cord midline.

Ex vivo spinal cord preparation

An *ex vivo* spinal cord was prepared according to our previous description (Szucs et al., 2009; Pinto et al., 2010). Briefly, the vertebral column was quickly cut out and immersed in oxygenated artificial cerebrospinal fluid at room temperature. The entire lumbosacral cord with bilateral L5 dorsal roots was dissected, and the pia mater was removed in the region of interest with forceps and scissors, to provide access for the recording pipettes. The spinal cord was glued with cyanoacrylate adhesive to a plate made of gold (the dorsolateral surface was up) and transferred to the recording chamber. All recordings were performed at 22–24°C to

better preserve neural network viability (Szucs et al., 2009). Lamina I neurons were visualized in the region between the dorsolateral funiculus and the dorsal root entry zone (Pinto et al., 2010) using the oblique infrared light-emitting-diode (OSRAM, SFH 4550, 850 nm) illumination technique (Safronov et al., 2007; Szucs et al., 2009). Lamina I neurons could be clearly distinguished from deeper located Lamina II neurons because of their larger and more loosely packed somata (Szucs et al., 2009).

Recording

Whole-cell recordings were conducted from the neurons in the lumbar segments L4–L6. Artificial cerebrospinal fluid contained (in mM): 115 NaCl, 3 KCl, 2 $CaCl_2$, 1 $MgCl_2$, 1 NaH_2PO_4, 25 $NaHCO_3$, and 11 glucose (bubbled with 95% O_2/5% CO_2). The pipettes were pulled from thick-walled glass (BioMedical Instruments) and fire-polished (resistance, 4–6 MΩ). The pipette solution contained (in mM): 3 KCl, 150 K-gluconate, 1 $MgCl_2$, 1 BAPTA, and 10 HEPES (pH 7.3 adjusted with KOH, final K^+ concentration of 160 mM). For *post hoc* characterization of recorded neurons, 0.5% biocytin was added to the internal solution. We used an EPC10-Double amplifier (HEKA) with a low-pass filter set at 2.9 kHz and a sample rate set at 10 kHz. Offset potentials were compensated before seal formation. Liquid junction potentials were calculated and corrected for in all experiments using the compensation circuitry of the amplifier. Bicuculline was applied by bath perfusion. Unless otherwise stated, all chemicals were obtained from Sigma-Aldrich.

The contralateral DRPs (cDRPs) were recorded with a suction electrode placed on the L5 root near to its entrance to the spinal cord. Each suction electrode had its own reference electrode. For recording, we used the differential AC amplifier (1700, A-M Systems), in which the low cutoff filter was either set to 0.1 Hz or open to allow the DC recording. The signal was digitized using the A/D converter of the patch-clamp amplifier. The cDRPs were evoked at 10-s intervals (Fernandes et al., 2020).

Primary afferent inputs were evoked by stimulating ipsilateral and contralateral L5 dorsal roots via suction electrodes using isolated pulse stimulators (2100, A-M Systems) as described previously (Pinto et al., 2008, 2010). The suction electrodes were fabricated from the thick-walled glass (BioMedical Instruments) and fire-polished to fit the diameter of the roots. A 50-μs pulse of 100 or 150 μA was applied to recruit Aβ-fibers and Aδ-fibers (Aβδ), a 1-ms pulse of 100 or 150 μA to activate all Aβδ-fibers and C-fibers (Aβδ/C), and a 1-ms pulse of inverted polarity (−100 or −150 μA) was used for selective activation of C-afferents (Fernandes et al., 2018, 2020). EPSCs mediated by contralateral afferents (contralateral EPSCs) were considered as monosynaptic if they showed a low failure rate (max. three failures in 10 consecutive episodes) and a small latency variation (<1 ms). The afferent conduction velocity (CV) was calculated by dividing the conduction distance by the conduction time. The former included the length of the dorsal root from the opening of the suction electrode to the entry zone (range, 3.5–7.45 mm) and the estimated pathway within the spinal cord (range, 0.5–1.8 mm). The spinal pathway was measured from video images and calculated as the sum of the rostrocaudal and mediolateral distances between the cell body and the corresponding contralateral dorsal root entry zone. The conduction time was calculated for a monosynaptic EPSC from its latency with a 1-ms allowance for synaptic transmission.

The contralateral EPSCs were considered as mediated by C-fibers (C-EPSCs) if evoked by a 1-ms pulse and the estimated afferent CV was <0.5 m/s. When evoked by the inverted 1-ms pulse, the C-EPSC showed an increase in its latency by ~3 ms; this time was additionally subtracted when calculating the corresponding afferent CV (Fernandes et al., 2018). The contralateral EPSCs were considered as Aδ-fiber-mediated (Aδ-EPSCs) if evoked by a 50-μs pulse and the afferent CV was >0.7 m/s. Some EPSCs evoked by the ipsilateral root stimulation (ipsilateral EPSCs) at the Aβδ-fiber strength (50 μs × 100 μA) were mediated by the afferents with the C-fiber range CVs; they were classified as the low-threshold C-EPSCs.

The afferent-driven presynaptic inhibition was examined by analyzing alterations in the magnitude of the monosynaptic EPSCs using inverted-pulse and paired-pulse protocols. For the contralateral afferents, we applied the inverted-pulse protocol (Fernandes et al., 2020) to record an increase in the monosynaptic C-EPSCs after removal of the Aβδ-fiber-driven presynaptic inhibition. To study interactions between contralateral and ipsilateral afferents, we used the paired-pulse protocol and analyzed reduction in the amplitude of the monosynaptic ipsilateral EPSC after the conditioning stimulation of the contralateral root (Fernandes et al., 2022a). The interval between the paired pulses was set to 100 ms based on our recordings of cDRPs. The input was considered as affected by the presynaptic inhibition if at least one component of the monosynaptic EPSC was reduced by the conditioning.

The reduction of the overall, mono- plus polysynaptic, ipsilateral EPSCs after contralateral conditioning was studied by the paired-pulse protocol. For each neuron, the EPSC integrals calculated for individual traces in control and after conditioning were compared by unpaired Student's *t* test and the difference was considered significant when $p < 0.05$. For the neurons showing significant effect, the percentage of the reduction is given as mean ± SEM. It should be noted that in some neurons contralateral conditioning evoked presynaptic inhibition of the monosynaptic ipsilateral EPSC component, but had no significant effect on the integral of the overall EPSC.

Lamina I neurons in the *ex vivo* spinal cord preparation show diverse intrinsic firing properties (Luz et al., 2014, 2019; Fernandes et al., 2016). In this study, neurons continuously discharging spikes at zero current injection were classified as rhythmic (Li and Baccei, 2011; Luz et al., 2014) and neurons with all other firing patterns were collectively termed as nonrhythmic.

Experimental design and statistical analysis

Data sets were compared using paired and unpaired Student's *t* tests and the difference was considered statistically significant when $p < 0.05$. All values are presented as mean ± SEM.

Results

Contralateral projections of primary afferents

First, we traced spinal projections of lumbar afferents by injecting a viral vector pAAV-CAG-tdTomato in the sciatic nerve. This induced expression of tdTomato in the corresponding DRG neurons (Fig. 1*A*) and their central terminals (Fig. 2). The tdTomato-expressing axons were analyzed in the contralateral dorsal horn in the lumbar segments L4–L6. We observed occasional primary afferent branches that crossed the spinal cord midline in the dorsal commissure and ran across the base of the contralateral dorsal horn (Fig. 2*A*,*B*). Some of these collaterals seemed to originate from the medial aspect of the dorsal horn where labeled afferents entered the gray matter (Fig. 2*A*), while some others started their contralateral projections from the lateral dorsal horn (Fig. 2*B*). A total of 36 midline crossings were observed in 38 spinal cord cross-sections of 100-μm thickness each. Since tdTomato expression was only induced in a fraction of DRG neurons (Fig. 1), this amount of the midline crossings was considered as a low estimate of the number of decussating afferents.

Thin tdTomato-expressing fibers with bouton-like enlargements were observed stretching along the dorsal surface of the contralateral dorsal horn in the termination zone of the ipsilateral CGRP-positive and IB4-positive primary afferents (Fig. 2*C*, *D*). Moreover, the contralateral afferents were found in close apposition to the primary afferent terminals positive for CGRP and IB4 (Fig. 2*D1–D3*). The tdTomato-expressing varicosities were also seen to contact mediolaterally-oriented dendrites and somata (labeled by anti-MAP2 and Nissl stain, respectively) of Lamina I neurons (Fig. 2*E1–E3*) and deeper located Lamina II neurons (Fig. 2*F1–F3*,*G1–G3*).

These experiments have shown that lumbar afferent fibers project to the contralateral dorsal horn and reach neurons in the

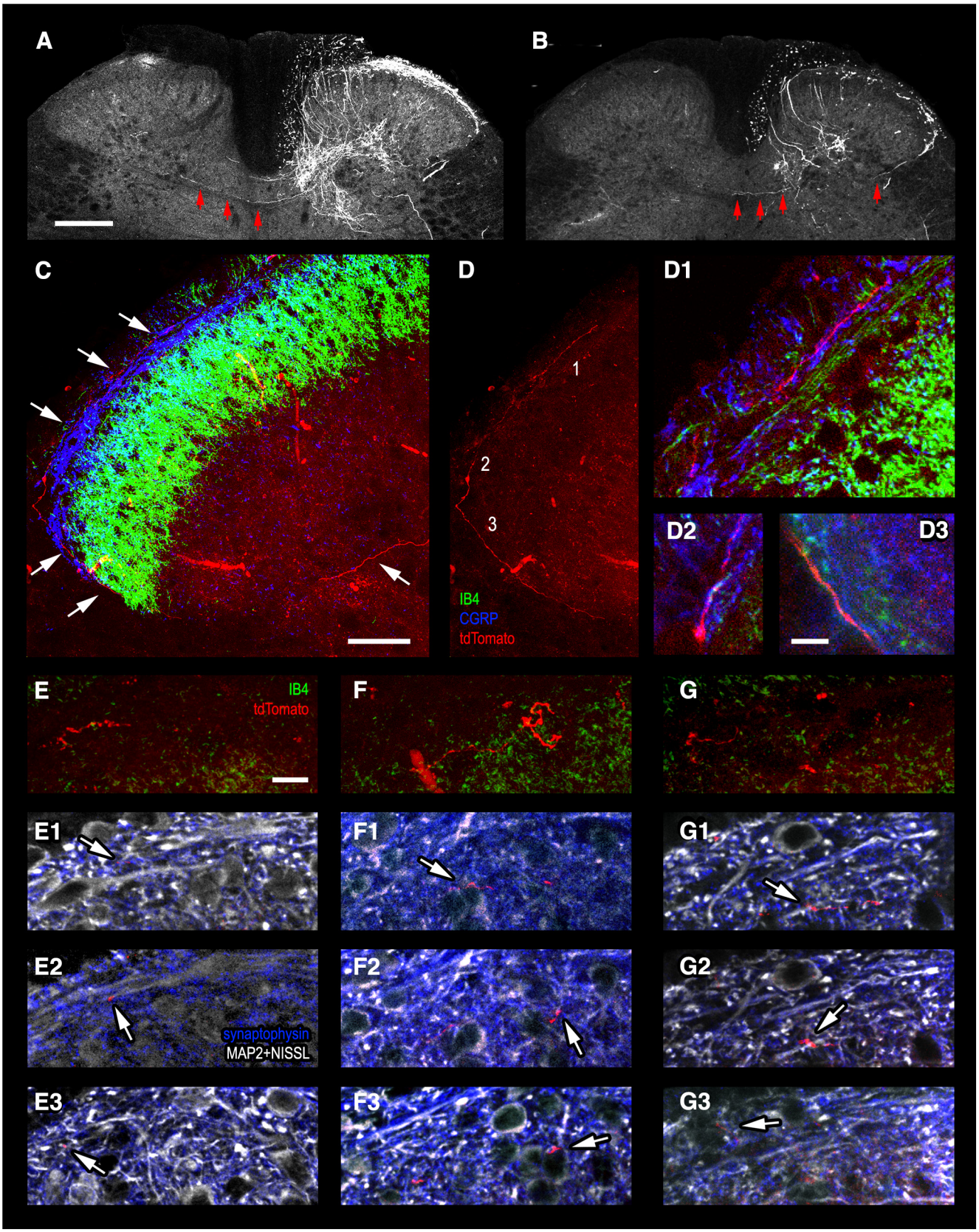

Figure 2. Tracing projections of primary afferent fibers to the contralateral superficial dorsal horn. ***A***, ***B***, Low-magnification confocal images showing tdTomato-expressing primary afferent collaterals crossing the spinal cord midline in the dorsal commissure and running toward the contralateral dorsal horn (three arrows). ***A***, Collateral originating from the medial aspect of the dorsal horn where tdTomato-expressing afferents enter the gray matter. ***B***, Collateral arising from the lateral dorsal horn (single arrow). ***C***, ***D***, A thin primary afferent collateral (red) with bouton-like enlargements stretches along the dorsal surface of the contralateral dorsal horn (white arrows) in the termination zone of CGRP-positive (blue) and IB4-positive (green) afferents. The images are Z-projections of 81 single 0.5-μm-thick optical sections. ***D1–D3***, Regions 1–3 from ***D*** are given at higher magnification to show close appositions of the tdTomato-expressing

superficial laminae. Close appositions of the contralateral fibers and their varicosities to Lamina I and II neurons suggested existence of functional synapses.

Contralateral primary afferent input to Lamina I neurons

In order to test whether primary afferent fibers functionally supply contralateral Lamina I neurons, we did whole-cell recordings using the *ex vivo* spinal cord preparation with bilaterally preserved L5 dorsal roots (Fig. 3*A*). Responses to stimulations of both roots were tested in 196 neurons located in the lateral half of Lamina I (84 animals). We applied saturating stimuli activating all groups of afferents (A$\beta\delta$/C) to evaluate the overall, mono- plus polysynaptic, EPSCs. A majority of the neurons ($n = 134$, i.e., 68.4%; 73 animals) received only ipsilateral input, whereas 62 neurons (i.e., 31.6%; 43 animals) showed both ipsilateral and contralateral primary afferent inputs. The neurons with bilateral input were all located in the lateral third of Lamina I. In 53 of them (27.0% of the total population), the contralateral root stimulation evoked EPSCs (Fig. 3*A*), whereas the remaining 9 neurons showed only small IPSCs (not shown). The amplitude of the contralateral EPSCs ranged from 7 to 310 pA (the mean, 52.3 ± 8.7 pA; $n = 53$; Fig. 3*B*). In 30 of these 53 neurons, the ipsilateral EPSCs were not distorted by uncontrolled discharges of the voltage-gated Na^+ currents, and therefore, the amplitudes of the ipsilateral and contralateral inputs could be compared (Fig. 3*C*). The mean contralateral EPSC was significantly smaller than the ipsilateral one (57.5 ± 14.6 vs 301.3 ± 52.9 pA, respectively, $n = 30$, $p < 0.0001$, paired *t* test; Fig. 3*C*, left). In this sample, the ratio between the amplitudes of contra and ipsilateral EPSCs in individual neurons ranged from 0.02 to 1.8 (mean 0.36 ± 0.07, $n = 30$; Fig. 3*C*, right).

We next asked whether Lamina I neurons receiving contralateral input could be distinguished from those lacking it on the basis of the magnitude of their ipsilateral input. For this, the ipsilateral EPSCs in 30 neurons from Figure 3*C* were compared with those in randomly selected 30 cells receiving only ipsilateral input. These amplitudes did not show a significant difference (301.3 ± 52.9 pA, $n = 30$; for the neurons with bilateral input vs 256.7 ± 33.4 pA, $n = 30$; for the neurons with ipsilateral input only; $p = 0.48$, unpaired *t* test). Thus, Lamina I neurons involved in the bilateral processing have their ipsilateral input similar to that of the neurons processing only ipsilateral information.

Monosynaptic contralateral input

In 17 Lamina I neurons located in segments L4–L6, some components ($n = 23$) of the contralateral input showed low failure rates and small latency variations and could be characterized as monosynaptic (Fig. 3*D*). Twenty of them were mediated by the afferents with the C-fiber-range CV (C-EPSCs), and three by the faster conducting Aδ-fibers (Aδ-EPSCs). Using *post hoc* biocytin histochemistry, we have identified five cells with contralateral monosynaptic inputs as PNs and one as an LCN. The PNs had their major axon crossing the spinal cord midline in the anterior commissure, whereas the axon of the LCN branched extensively within the ipsilateral dorsal horn and did not cross the spinal cord midline. According to their intrinsic firing properties, 11 neurons with a monosynaptic input, including all five identified PNs, were nonrhythmic, whereas the remaining six neurons were rhythmic, i.e., continuously discharged spikes at zero current injection (Li and Baccei, 2011; Luz et al., 2014). According to our previous studies, the vast majority of Lamina I rhythmic neurons are LCNs (Luz et al., 2014; Fernandes et al., 2016) and express two major markers of inhibitory neurons, VGAT (Szucs et al., 2013) and Pax2 (Fernandes et al., 2022b). Therefore, it could be concluded that thin primary afferents can directly supply contralateral Lamina I PNs and LCNs, some of which being putative inhibitory interneurons.

Inhibitory gate control of the contralateral input

In the following experiments we tested whether the presynaptic and postsynaptic forms of feedforward inhibition control contralateral primary afferent input and whether disinhibition of these circuits can increase excitatory drive to Lamina I neurons.

First, we compared monosynaptic inputs evoked by the contralateral primary afferent volleys activated by a 1-ms pulse of normal polarity (activating all A$\beta\delta$/C-fibers) and inverted polarity (activating only C-fibers; Fernandes et al., 2018, 2020). This allowed us to estimate how the contralateral C-fiber input is affected by the presynaptic inhibition driven by the faster conducting contralateral A$\beta\delta$-fibers (Fernandes et al., 2020). An appearance of a new monosynaptic EPSC component, as a result of removal of the presynaptic inhibition, was seen in eight neurons. In five of them, a new component appeared in addition to an already existing one (Fig. 4*A1*). This implied that these neurons were directly supplied by several contralateral afferent fibers, some of which are subject to the afferent-driven presynaptic inhibition and others not. In the remaining three cases, the inverted pulse stimulation revealed a new monosynaptic component of input in a neuron responding only with a polysynaptic EPSCs to the normal pulse stimulation (Fig. 4*A2*); these neurons were only supplied by the C-fibers controlled by the presynaptic inhibition. Therefore, disinhibition of the afferent-driven presynaptic circuitry can increase direct excitatory synaptic drive to the contralateral Lamina I.

To reveal the effect of the network disinhibition on the contralateral input, we selected neurons in which the stimulus inversion did not increase response and studied its change in the presence of the $GABA_A$ receptor blocker bicuculline (20 μM). The effect of disinhibition was seen in seven of nine neurons tested. In five of them (three identified as PNs and one as an LCN), the contralateral polysynaptic input substantially increased in the presence of bicuculline (Fig. 4*B1*), implying disinhibition of the neuronal network processing contralateral input. In two neurons, the effect of bicuculline was seen as an increase in the polysynaptic input and appearance of a new monosynaptic EPSC component (Fig. 4*B2*). In the remaining two neurons, both identified as PNs, bicuculline did not change the contralateral input. Therefore, the network disinhibition is likely to produce both postsynaptic and presynaptic effects.

Thus, our experiments have shown that presynaptic and postsynaptic forms of feedforward inhibition control contralateral afferent input, and that the dorsal horn network disinhibition can increase contralateral excitatory drive to Lamina I neurons.

←

afferent (red) with CGRP-positive (blue) and IB4-positive (green) primary afferent terminals (Z-projections from 2–6 optical sections). ***E–G***, tdTomato-expressing primary afferent collateral fragments with varicosities (red) near the termination zone of IB4-positive (green) primary afferents. Z-projections from 10–20 optical sections. ***E1–E3***, ***F1–F3***, ***G1–G3***, Single optical sections showing tdTomato-expressing primary afferent varicosities contacting (arrows) elongated mediolaterally-oriented MAP2-positive dendrites of Lamina I neurons (white, ***E1–E3***), as well as Nissl-stained somata (white, ***F1–F3***) and MAP2-positive dendrites (white, ***G1–G3***) of Lamina II neurons. Scale bars: 200 μm in ***A*** (the same in ***B***), 50 μm in ***C*** (the same in ***D***), 10 μm in ***D1–D3*** and ***E–G*** (the same in ***E1–E3***, ***F1–F3***, and ***G1–G3***).

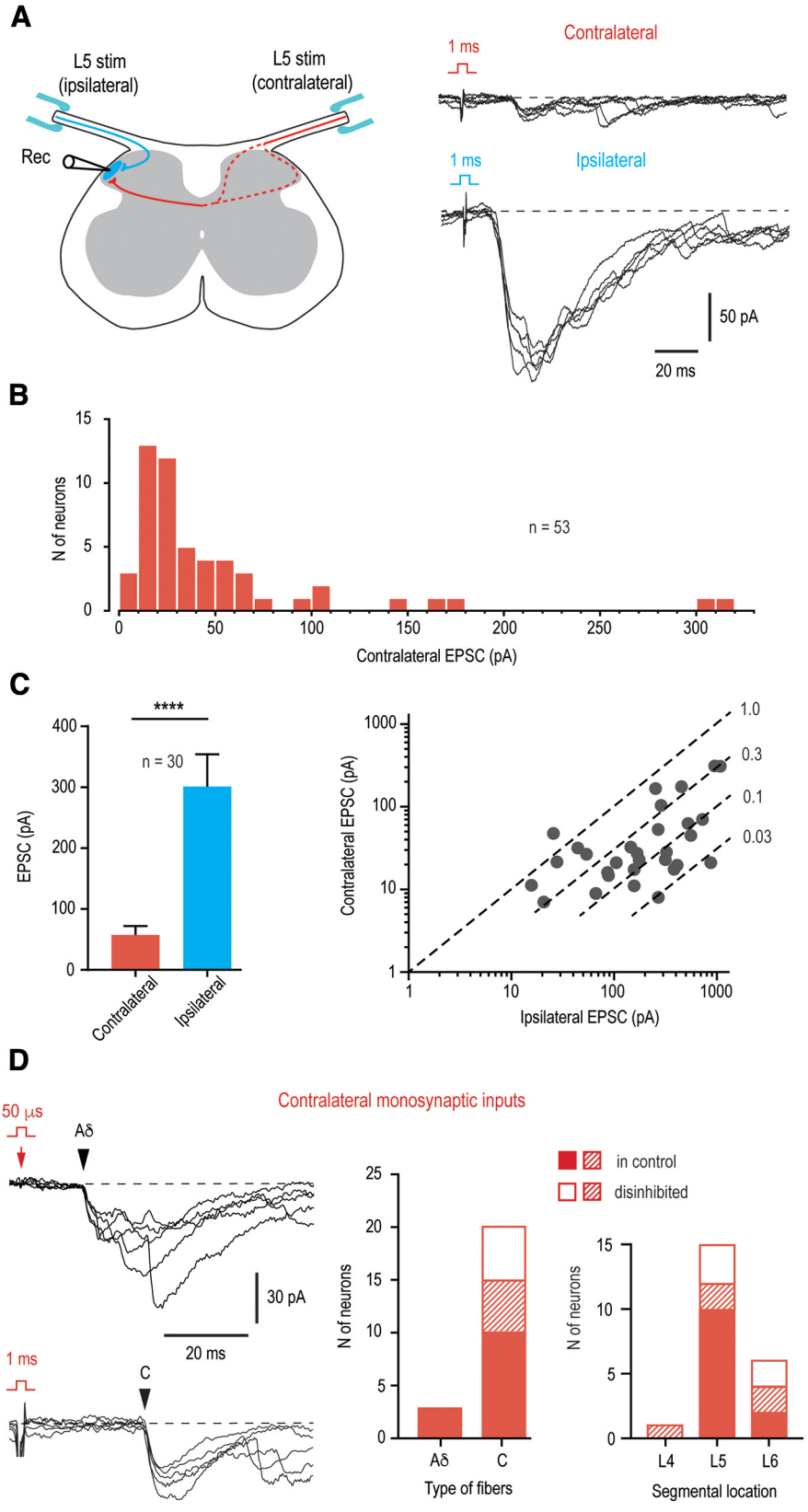

Figure 3. Contralateral Aδ-fiber and C-fiber input to lumbar Lamina I neurons. ***A***, Left panel, Schematic of the experimental design used to study ipsilateral (blue) and contralateral (red) primary afferent input to a Lamina I neuron. Note that decussating thin afferent collaterals can run via medial or lateral dorsal horn (dashed lines). Right, Overall mono- plus polysynaptic EPSCs evoked in an L5 Lamina I neuron after stimulating contralateral and ipsilateral L5 dorsal roots at intensity activating all Aβδ/C-fibers (5 traces each). Holding potential, −80 mV. ***B***, Distribution of the amplitudes of the overall EPSCs evoked by the contralateral dorsal root stimulation in 53 Lamina I neurons. ***C***, Comparison of the overall EPSCs evoked by contralateral and ipsilateral stimulation in neurons with bilateral input. Only Lamina I neurons with undistorted ipsilateral input were selected ($n = 30$). ****$p < 0.0001$, paired t test. Right, EPSC amplitudes for each of 30 neurons are plotted in double logarithmic coordinates. Dashed lines are shown for the ratios between the amplitudes of the contralateral and ipsilateral inputs of 1.0, 0.3, 0.1, and 0.03. ***D***, Monosynaptic Aδ-EPSC and C-EPSC components (indicated by arrowheads) of the contralateral input (5 traces each). Holding potential, −70 mV. The neuron receiving the Aδ-input was from the segments L6. The neuron receiving monosynaptic C-fiber input was located in the segment L5 and identified as a PN. Right, Histograms show the number of neurons with Aδ-fiber and C-fiber input and segmental locations of Lamina I neurons with direct contralateral input. Filled bars, neurons showing monosynaptic input in control; open bars, neurons that showed monosynaptic components only after attenuation of the afferent-driven presynaptic inhibition or disinhibition of the dorsal horn network (Fig. 4); crosshatched bars, neurons showing both monosynaptic input in control and a new component appearing after removal of inhibition.

Disinhibition boosts the efficacy of contralateral input

To study the functional implications of disinhibition on the contralateral afferent input to Lamina I neurons, we did current-clamp recordings. The ability of the contralateral synaptic drive to evoke action potential discharge was examined in control and in the presence of 20 μM bicuculline. These recordings were done from a diverse population of Lamina I neurons ($n = 14$, not included in the previous statistics; eight animals), which received excitatory ($n = 5$), inhibitory ($n = 2$), or no ($n = 7$) contralateral afferent input. We counted the total number of action potentials that were evoked by 10 consecutive stimulations (3-s intervals, 850-ms time windows analyzed).

In four of five neurons with the contralateral excitatory input, disinhibition significantly increased its efficacy (Fig. 5*A*). Under control conditions, these neurons showed contralateral EPSCs with amplitudes of 16, 21, 26, and 54 pA. The mean number of elicited action potentials in this group of neurons was 0.5 ± 0.3 in control, and increased to 10.2 ± 2.9 in the presence of bicuculline ($n = 4$, $p < 0.05$, paired t test; Fig. 5*A*). In the remaining neuron with the contralateral excitatory input (EPSC of 6 pA), spikes could be evoked neither in control nor in the presence of bicuculline.

Interestingly, the disinhibition-induced appearance of spike firing on the contralateral root stimulation was observed in two of two neurons with the contralateral inhibitory input and in five of seven neurons with no contralateral input (Fig. 5*B*). In this mixed population of Lamina I neurons, the number of action potentials increased from 0 in control to

15.7 ± 5.0 in the presence of bicuculline ($n = 7$, $p < 0.01$, paired t test). It should be noted that, when recorded in bicuculline, the subthreshold sweeps were interspersed with sweeps showing action potential discharges that lasted several hundred milliseconds. It is therefore likely that a broad disinhibition of the dorsal horn network played a key role in boosting efficacy of the contralateral input. In the remaining two neurons without contralateral input in control, small evoked polysynaptic EPSPs appeared after application of bicuculline, however, they remained subthreshold and did not trigger spike discharges.

Thus, one could conclude that the spinal network disinhibition affects decussating pathways and boosts the efficacy of contralateral afferents in excitation of Lamina I neurons. Furthermore, network disinhibition can open a gate allowing contralateral excitatory synaptic drive to reach neurons that under normal conditions receive inhibitory or no contralateral afferent input.

Contralateral control of the ipsilateral input

As next, we asked whether the contralateral afferents, which do not supply a given Lamina I neuron, can presynaptically inhibit its ipsilateral input. Presynaptic inhibition is caused by the primary afferent depolarization (PAD) induced by Cl^- efflux through anion channels of $GABA_A$ receptors (Rudomin and Schmidt, 1999; Willis, 1999). The antidromic spread of PAD along the afferent fiber to the dorsal root can be recorded as a DRP (Barron and Matthews, 1938; Lloyd and McIntyre, 1949). Therefore, we first studied induction of the contralateral PAD in our preparation by recording contralateral DRPs (cDRPs). Stimuli activating only Aβδ-afferents, only C-afferents, and all Aβδ/C-afferents were applied to an L5 dorsal root, while recording the cDRPs from the contralateral L5 root (Fig. 6*A*). In six spinal cords tested, activation of Aβδ-afferents, C-afferents, and Aβδ/C-afferents evoked Aβδ-cDRP, C-cDRP and Aβδ/C-cDRP, respectively (Fig. 6*A*). After the stimulation, the peak of the response was reached at 102 ± 6 ms for Aβδ-cDRP ($n = 6$), 108 ± 7 ms for C-cDRP ($n = 4$), and 98 ± 6 ms for Aβδ/C-cDRP ($n = 6$). Bicuculline at a 20 μM concentration virtually completely suppressed Aβδ-cDRP, Aβδ/C-cDRP (Fig. 6*A*) and C-cDRP (not shown, $n = 6$). Based on these experiments we could conclude that both Aβδ-afferents and C-afferents

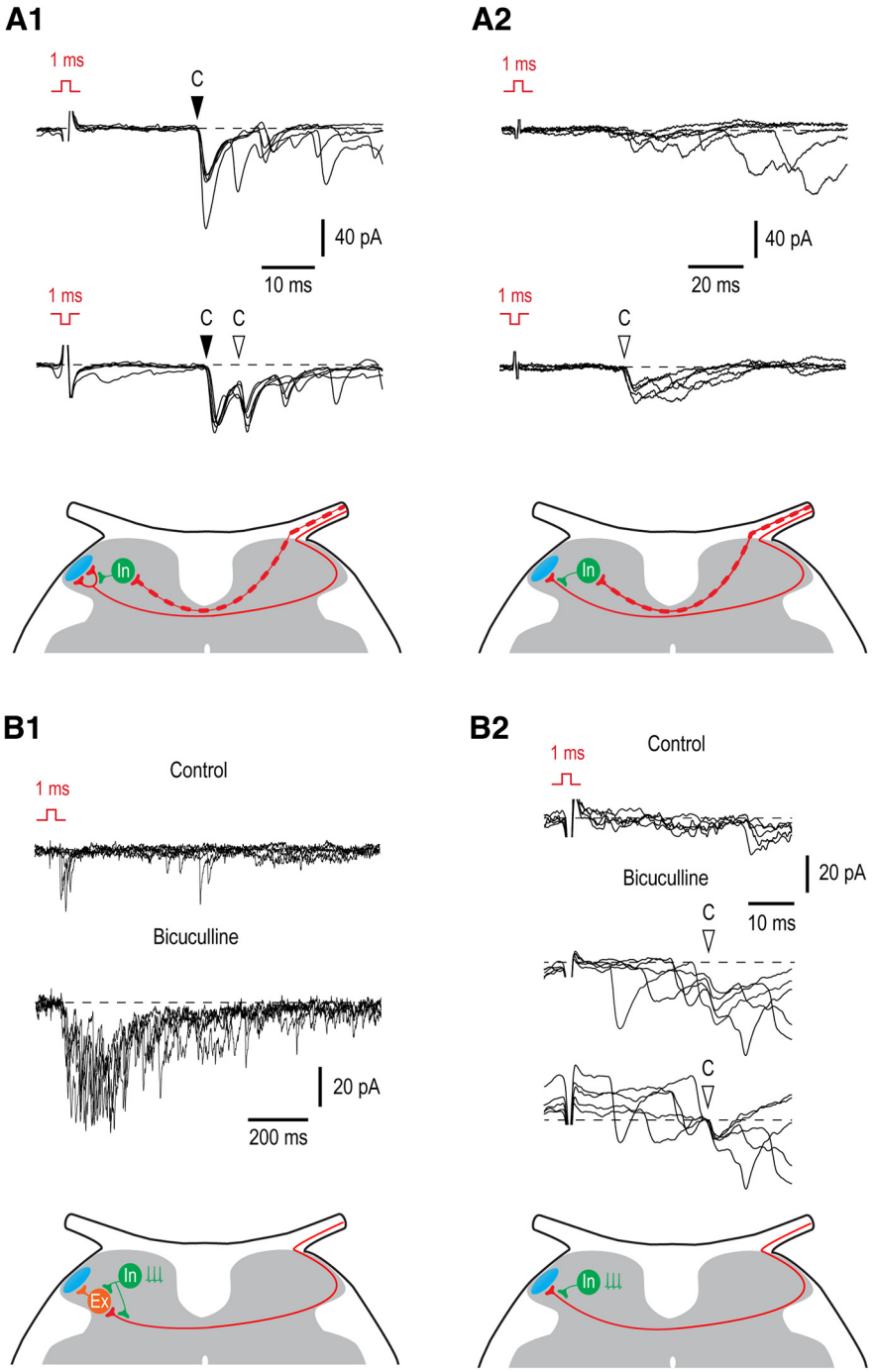

Figure 4. Inhibitory control of the contralateral input. ***A1***, ***A2***, Afferent-driven presynaptic inhibition of the monosynaptic C-fiber input to Lamina I neurons. ***A1***, Recording from a neuron in which attenuation of the Aβδ-fiber-driven presynaptic inhibition by the inverted pulse stimulation resulted in an appearance of a new monosynaptic C-EPSC (open arrowhead) in addition to the component seen in control (filled arrowhead). Schematic shows a phasic Aβδ-fiber-mediated presynaptic inhibition at one of two contralateral C-fiber branches supplying Lamina I neuron. ***A2***, Removal of the Aβδ-afferent-driven presynaptic inhibition unblocks a monosynaptic C-fiber input (open arrowhead). Schematic shows a phasic presynaptic inhibition at the contralateral C-fiber branch supplying Lamina I neuron. ***B1***, ***B2***, Network disinhibition by bicuculline (20 μM) increases the contralateral input to Lamina I neurons. ***B1***, Disinhibition augments the polysynaptic input. Schematic, an increase in the polysynaptic input can be caused by removal of a tonic postsynaptic inhibition from excitatory interneuron or from the presynaptic terminal of the afferent supplying this interneuron. ***B2***, Network disinhibition unblocks contralateral monosynaptic C-fiber input (open arrowhead) to an LCN. In bicuculline, the same family of traces is also shown below with membrane currents at the time point of the monosynaptic EPSC initiation shifted to the same level. Schematic, a tonic presynaptic inhibition at the contralateral C-fiber branch supplying Lamina I neuron. Holding potential was −70 mV in ***A1***, ***B1***, and ***B2***, and −80 mV in ***A2***. For each type of response, five traces are shown. Locations of inhibitory (In) and excitatory (Ex) interneurons are not known.

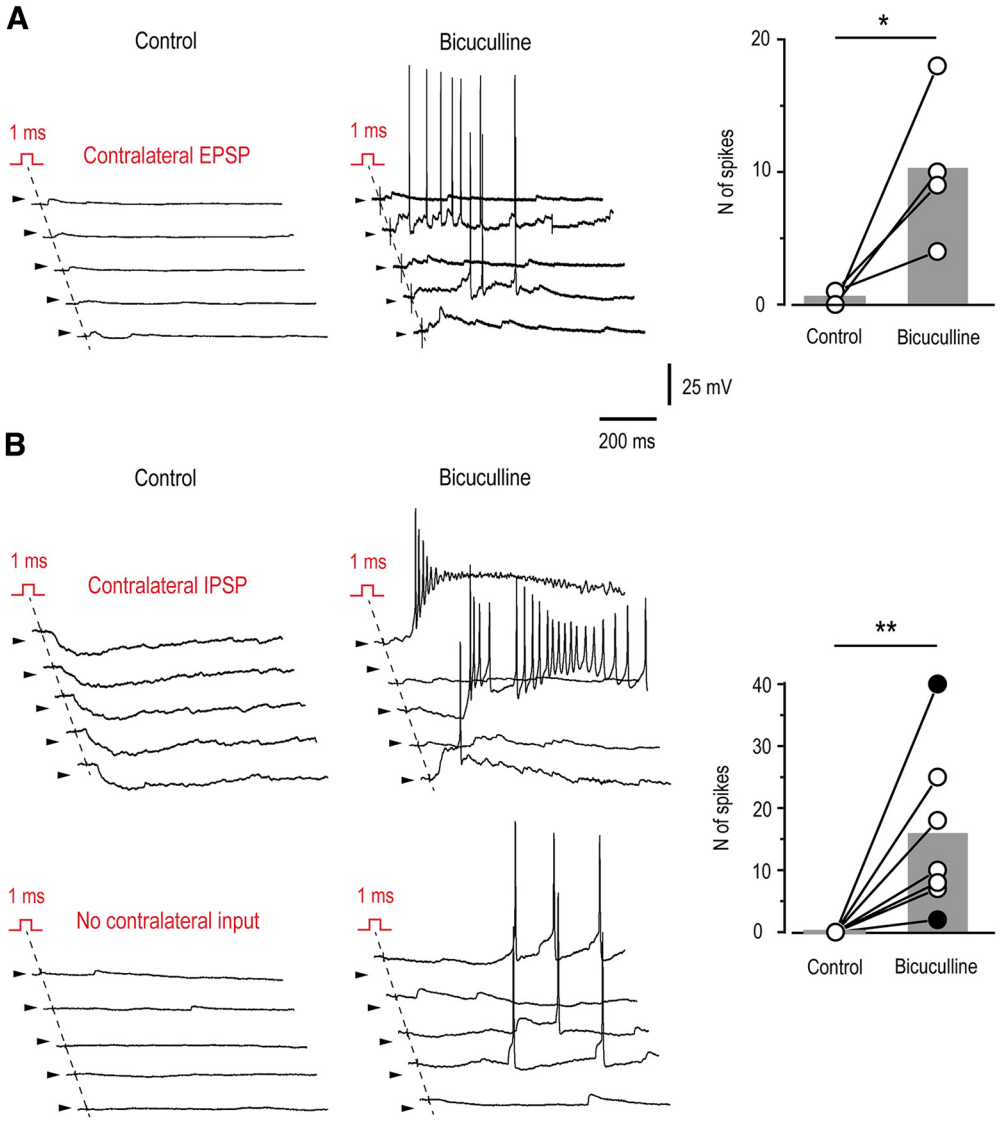

Figure 5. Network disinhibition increases efficacy of the contralateral afferent input. Current-clamp recordings done in control and in the presence of 20 μM bicuculline from Lamina I neurons receiving excitatory (EPSC of 16 pA; ***A***), inhibitory or no (***B***) contralateral input. Right, Numbers of spikes evoked by 10 consecutive stimulations of the contralateral dorsal root are plotted for individual neurons. Gray bars indicate the mean value for each cell group. Neurons with inhibitory (filled symbols) or no (open symbols) contralateral input are presented as one group. In all traces, arrowheads indicate a potential of −70 mV. *$p < 0.05$, **$p < 0.01$; paired *t* test.

induce a $GABA_A$-receptor-mediated contralateral PAD, and can evoke presynaptic inhibition of the contralateral primary afferent system.

Therefore, we tested whether the contralateral afferents induce a presynaptic inhibition of the ipsilateral input to Lamina I (Fig. 6*B*,*C*). For this, we did the whole-cell recordings from 20 Lamina I neurons with a monosynaptic ipsilateral supply. In five of them (one identified as a PN), the contralateral conditioning suppressed seven monosynaptic EPSC components. The contralateral A$\beta\delta$-range conditioning affected ipsilateral Aδ-EPSCs ($n = 2$; Fig. 6*B*,*C*) and low-threshold C-EPSCs ($n = 4$; Fig. 6*C*). In the remaining case, the contralateral C-fibers evoked an inhibition of an ipsilateral C-EPSC component ($n = 1$). The amplitude of these monosynaptic components was reduced by 78.9 ± 9.8% ($n = 7$).

In these 20 neurons, we also analyzed an effect of the contralateral conditioning on the integral of the ipsilateral overall, monosynaptic plus polysynaptic, response (Fig. 7). This gave us an estimate of the total inhibitory effect produced by the contralateral afferents. A significant reduction in the EPSC integral was revealed in seven neurons (one identified as a PN and two as LCNs). The contralateral A$\beta\delta$-range conditioning reduced the ipsilateral A$\beta\delta$-EPSCs ($n = 3$; Fig. 7*A*) and A$\beta\delta$/C-EPSCs ($n = 1$) by 53.2 ± 10.9% ($n = 4$). The contralateral A$\beta\delta$/C-range conditioning reduced the ipsilateral A$\beta\delta$-EPSCs ($n = 4$) and A$\beta\delta$/C-EPSCs ($n = 2$) by 39.7 ± 12.7% ($n = 6$). In three of these six cases, an increase in the contralateral conditioning stimuli from the A$\beta\delta$-range to A$\beta\delta$/C-range produced a significant reduction in the ipsilateral response mediated by A$\beta\delta$-afferents ($n = 1$; Fig. 7*B*) and A$\beta\delta$/C-afferents ($n = 2$). This additional effect caused by the contralateral C-fiber recruiting was 22.0 ± 1.5% ($n = 3$).

Thus, the major contralateral inhibition of both the monosynaptic and overall ipsilateral inputs to Lamina I neurons was driven by A$\beta\delta$-afferents.

Discussion

We used *ex vivo* spinal cord preparation to examine contralateral afferent input to Lamina I. Our main findings are: (1) lumbar afferents project to the contralateral superficial dorsal horn and

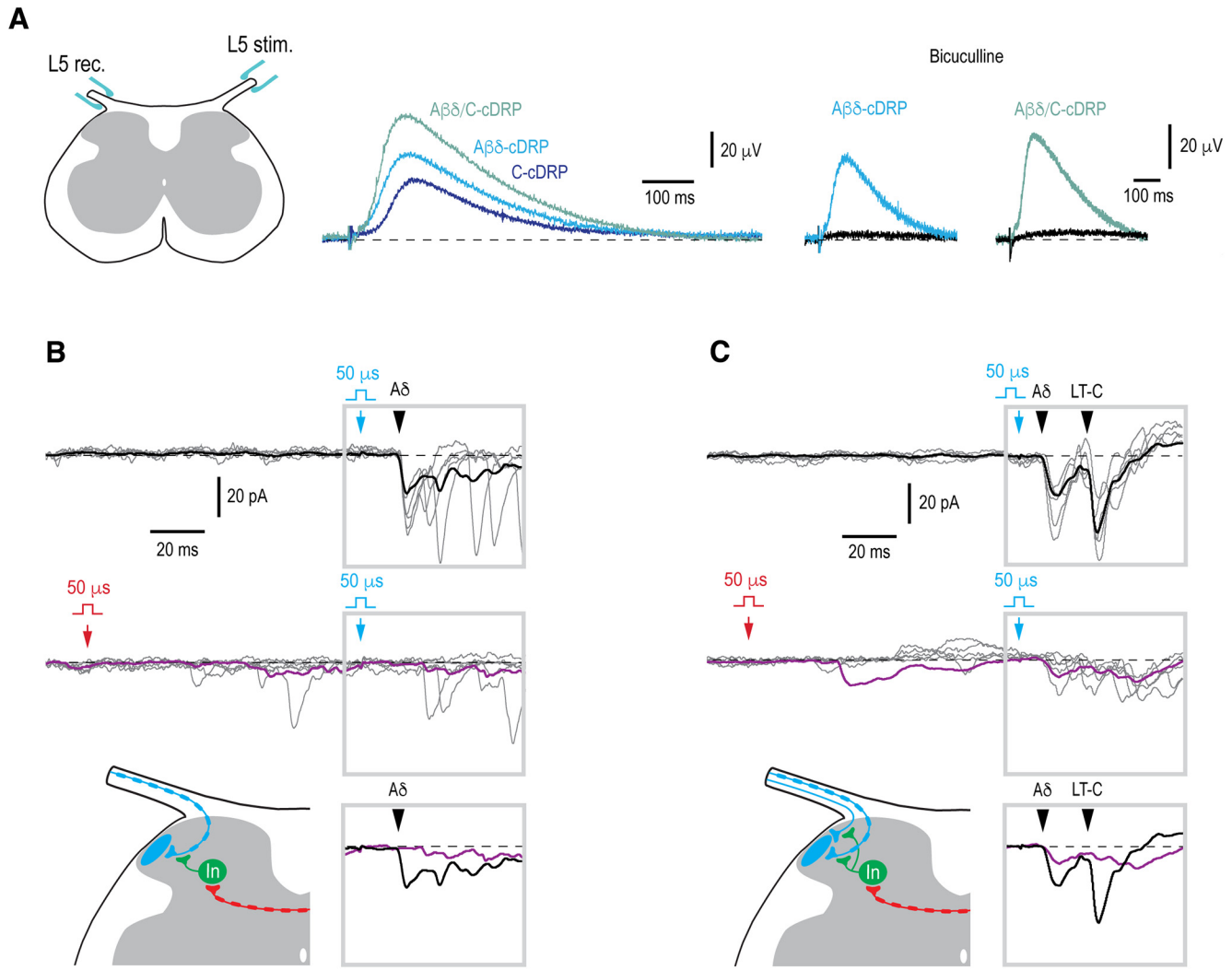

Figure 6. Contralateral control of the ipsilateral monosynaptic input. ***A***, Recording of the cDRPs. Left panel shows a schematic of how the cDRPs were recorded in the isolated spinal cord preparation. The recording electrode was placed on the contralateral L5 dorsal root close to where it entered the spinal cord. Middle, cDRPs evoked by stimulating Aβδ-afferents (Aβδ-cDRP), C-afferents (C-cDRP), and Aβδ/C-afferents (Aβδ/C-cDRP). Right, Bicuculline (20 μM) effect on the Aβδ-cDRP and Aβδ/C-cDRP. ***B***, Contralateral Aβδ-range conditioning abolished ipsilateral Aδ-EPSC component. Schematic, Contralateral Aβδ-afferent induces presynaptic inhibition of the ipsilateral Aδ-fiber input to a Lamina I neuron. ***C***, Contralateral Aβδ-conditioning attenuated the ipsilateral Aδ-EPSC and abolished the low-threshold-(LT)-C-EPSC. Schematic, a contralateral Aβδ-afferent induces inhibition of the ipsilateral Aδ- and LT-C-afferents. In ***B***, ***C***, 50-μs stimuli were applied to activate Aβδ-afferents or LT-C-afferents. Monosynaptic EPSCs are indicated by filled arrowheads. Holding potential, −80 mV. The time moments when conditioning (contralateral) and test (ipsilateral) stimuli were applied are indicated by red and blue arrows, respectively. For each type of response, five individual traces are shown with the average of 10–15 traces. Averaged responses to the test stimuli are shown superimposed below. Location of an inhibitory interneuron (In) is not known.

terminate in a close apposition to the somata and dendrites of Lamina I–II neurons, (2) functional synapses mediate direct input from decussating Aδ-afferents and C-afferents to Lamina I PNs and LCNs, (3) a substantial part of the contralateral drive reaches neurons via polysynaptic pathways, (4) the contralateral afferent input is under feedforward inhibitory control, (5) attenuation of the afferent-driven presynaptic inhibition or disinhibition of the spinal network increase contralateral input and its ability to excite neurons, and (6) contralateral afferents can control ipsilateral input to Lamina I. Therefore, disinhibition of the decussating afferent pathways targeting nociceptive PNs can be an important step in developing mirror-image pain.

Morphophysiology of contralateral input

Contralateral branches of thin afferents were mentioned in earlier reports (Culberson et al., 1979; Light and Perl, 1979a,b; Réthelyi et al., 1979). They cross the spinal cord midline in the dorsal commissure to terminate mostly in the contralateral laminae V and I. Functionally, some of them were classified as cutaneous Aδ-mechanical-nociceptors (Light and Perl, 1979b). Decussating thin afferents are abundant in the medullary, cervical, thoracic and sacral cord, but much less numerous in the lumbar segments (Culberson et al., 1979; Pfaller and Arvidsson, 1988; Marfurt and Rajchert, 1991). The number of the midline crossings observed here (~1 per 100-μm section) was close to the value reported for the lumbar cord (Light and Perl, 1979a). However, the true number of decussating afferents can be higher, since only a fraction of small DRG neurons became labeled after the sciatic injection of viral vector in our experiments. The fibers crossing the midline just dorsal to the central canal could also supply Lamina X neurons (Krotov et al., 2019, 2022).

We have found that the contralateral afferents bend repeating the curvature of the superficial dorsal horn being in a proximity to the termination fields of the ipsilateral peptidergic, CGRP-positive,

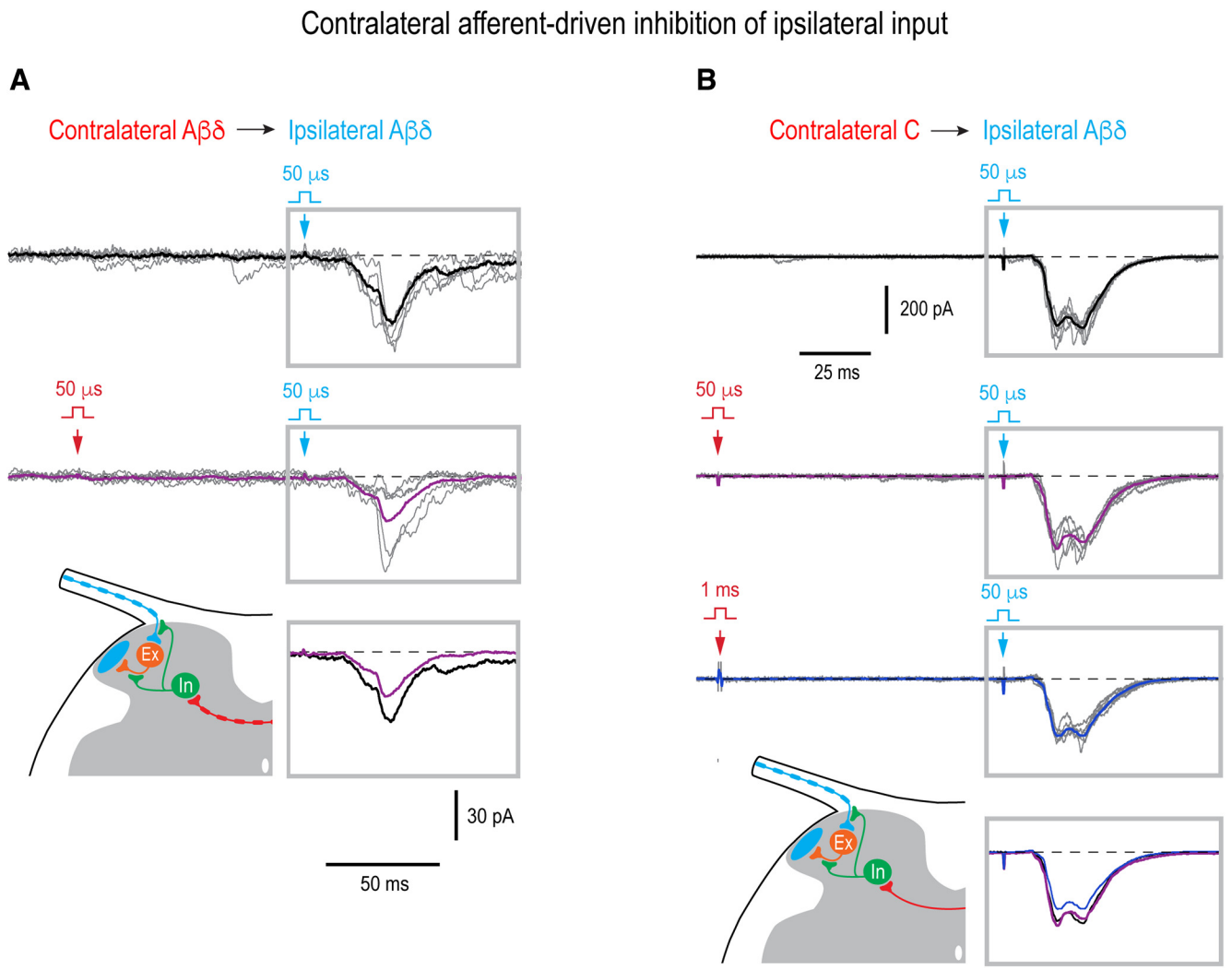

Figure 7. Contralateral control of the ipsilateral overall input. ***A***, Contralateral A$\beta\delta$-range conditioning attenuated the ipsilateral Aδ-fiber input in a PN (integral reduced by 55%, $p = 0.03$, unpaired t test). Holding potential, −70 mV. ***B***, Contralateral A$\beta\delta$-conditioning did not change the ipsilateral Aδ-fiber input ($p = 0.3$, unpaired t test) that was however significantly attenuated by the contralateral A$\beta\delta$/C-conditioning (integral reduced by 21%, $p < 0.001$, unpaired t test). Thus, the effect was considered to be driven by the contralateral C-afferents. Holding potential, −80 mV. In ***A***, ***B***, 50-μs stimuli were applied to activate A$\beta\delta$-afferents and 1-ms stimuli to activate all A$\beta\delta$/C-afferents. The time interval between the contralateral conditioning stimulus (red arrow) and ipsilateral test stimulus (blue arrow) was 100 ms. For each type of response, five traces are shown with the average of 7–21 traces. Averaged responses to the test stimuli are shown superimposed below. Schematics show contralateral A$\beta\delta$-afferent-driven (***A***) and C-afferent-driven (***B***) presynaptic inhibition of the ipsilateral afferent supplying an intercalated excitatory neuron or/and of the axon terminal of the intercalated neuron. The presynaptic, rather than postsynaptic, mechanism of the contralateral inhibition of the ipsilateral polysynaptic input was assumed, since effect was observed 100 ms after conditioning stimulation when cDRP, and therefore PAD, reached its maximum (Fig. 6*A*), but most evoked IPSCs already terminated (Luz et al., 2019; Fernandes et al., 2022a). Locations of inhibitory (In) and excitatory (Ex) interneurons are not known.

and nonpeptidergic, IB4-positive, nociceptors. The contralateral afferents contacted somatodendritic domains of Lamina I–II neurons. At least some synapses on Lamina I neurons, including PNs, are functional and mediate direct contralateral Aδ-afferent and C-afferent input. Lamina II neurons receiving contralateral supply could mediate the polysynaptic component of the input to Lamina I neurons. The polysynaptic component could also originate from a number of alternative sources, e.g., deep dorsal horn neurons receiving contralateral input (Fitzgerald, 1982, 1983), commissural interneurons (Petkó and Antal, 2000; Petkó et al., 2004) or commissural axon collaterals of Lamina I PNs (Kokai et al., 2022). For recordings, we used young animals (P13–P20), in which synaptic circuit maturation has not yet finished, and therefore, the overall strength of the primary afferent drive to contralateral Lamina I neurons can increase during development.

Inhibitory control

An interesting finding of this work is that the contralateral input is subject to diverse forms of inhibitory control and itself can affect the ipsilateral input to Lamina I.

The contralateral afferents interfere with each other via the mechanism of afferent-driven presynaptic inhibition, so that A$\beta\delta$-fibers control C-fiber input to Lamina I. This form of inhibition provides a phasic control of the information flow and can increase the noxious threshold for the contralateral receptive field. Furthermore, it can represent a mechanism restricting the size of the contralateral receptive fields of Lamina I neurons. Attenuation of the afferent-driven presynaptic inhibition can increase the contralateral drive to the neurons and the size of their receptive fields.

An increase in the contralateral polysynaptic response and an appearance of new monosynaptic components after network

disinhibition by bicuculline may implicate an important role of postsynaptic and presynaptic forms of tonic inhibitory control. This inhibition can be induced by rhythmic Lamina I LCNs (Luz et al., 2014; Fernandes et al., 2016) expressing major markers of inhibitory neurons (Szucs et al., 2013; Fernandes et al., 2022b). The tonic inhibition may prevent PNs from receiving contralateral nociceptive drive. As we show, the dorsal horn network disinhibition boosts the ability of contralateral input to excite Lamina I neurons. This can open a gate allowing contralateral afferent drive to reach those neurons that under normal conditions receive only inhibitory or no input.

We also show that contralateral afferents can evoke presynaptic inhibition of the ipsilateral afferents supplying Lamina I. It was caused by induction of the $GABA_A$-receptor-mediated PAD as evidenced by cDRP sensitivity to bicuculline. cDRPs were induced by both A$\beta\delta$-volleys and C-volleys, however, stronger effect on the ipsilateral input was produced by A$\beta\delta$-conditioning. Therefore, contralateral myelinated afferents can control ipsilateral inputs to nociceptive neurons.

Functional aspects

Commissural pathways linking the left and right sides of the spinal cord play a key role in bilateral processing of sensory information (Fitzgerald, 1982, 1983; Koltzenburg et al., 1999; Sotgiu et al., 2004). Here, we show that some lumbar Lamina I neurons receive direct contralateral afferent supply. These neurons were not specialized on the contralateral processing only as their ipsilateral input was significantly larger and not different from that in the neurons receiving only ipsilateral supply. Therefore, neurons with contralateral inputs can play a role in bilateral processing. This role may be related to their location in the lateral third of Lamina I. It is known that termination fields of primary afferents in the superficial dorsal horn are rigorously organized to form the somatotopic map of the body surface (Brown, 1982; Woolf and Fitzgerald, 1986; Warwick et al., 2022). The lateral third of the superficial dorsal horn at the L4–L6 level represents a termination field of cutaneous afferents innervating proximal dorsal areas, e.g., the low back, dorsocaudal surface of the hindlimb and perineum, while its most lateral part is targeted by the afferents innervating the dorsal midline of the limb (Takahashi et al., 2002, 2003). Thus, under physiological conditions, Lamina I neurons with contralateral input may be involved in the bilateral processing of sensory information arising from the proximal dorsal and axial body regions.

Pathologic implications

Processing mode of Lamina I neurons with bilateral input can change under pathologic conditions. Unilateral sciatic nerve lesion was shown to result in bilateral losses in inhibitory mechanisms within the dorsal horn (Ibuki et al., 1997; Simpson and Huang, 1998). Furthermore, it causes alterations in the contralateral expression of genes, receptors, ion channels and neuropeptides that can cause induction of the mirror-image pain (Koltzenburg et al., 1999). Mirror-image thermal hyperalgesia is mediated, at least in part, by neuropeptide substance P acting mainly on the neurokinin-1 receptor (Coderre and Melzack, 1991). Lamina I is likely to play a central role in this process, since both PNs and LCNs in this layer express the neurokinin-1 receptor (Al Ghamdi et al., 2009) and respond to substance P (Luz et al., 2014).

Our data suggest that mirror-image pain can be caused by an increase in the nociceptive drive to PNs because of attenuation of the contralateral inhibitory control (Fig. 8). Loss of the A$\beta\delta$-afferent-driven presynaptic inhibition of C-fibers (pathway 1) together with the spinal network disinhibition (pathway 2) can allow the ongoing afferent barrage in the injured nerve to reach the contralateral PNs. In this case, a PN on the uninjured side (blue) will be excited by the barrage arriving from the contralateral injured afferents (red) that will lead to a perception of pain

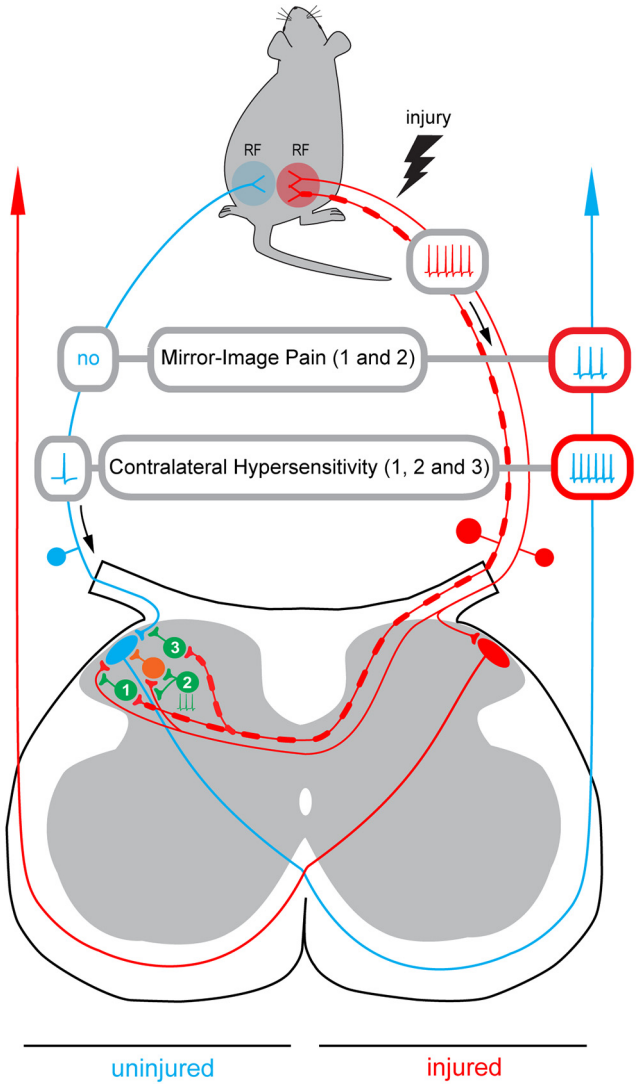

Figure 8. Induction of the mirror-image pain and contralateral hypersensitivity. Schematic illustrating how disinhibition of the decussating pathways can cause induction of the mirror-image pain. Based on our data, three inhibitory pathways are considered. Pathway 1, the contralateral A$\beta\delta$-afferent-driven presynaptic inhibition of the contralateral C-fiber input (Fig. 4*A1*,*A2*). Pathway 2, tonic network inhibition of the contralateral input (Fig. 4*B1*). The tonic inhibition of the C-fiber directly supplying Lamina I neuron is not indicated. Pathway 3, the contralateral A$\beta\delta$-afferent-driven presynaptic inhibition of the ipsilateral input (Fig. 6*B*, *C*). Disinhibition of pathways 1 and 2 will allow the ongoing afferent barrage in the injured nerve (red) to reach a Lamina I PN on the uninjured side (blue). Its excitation by the contralateral afferent barrage will result in a perception of pain as arising from the ipsilateral receptive field (RF) even if there is no activity in the ipsilateral afferents (Mirror-Image Pain). Disinhibition of pathway 3 will increase the ipsilateral afferent drive reaching a PN on uninjured side after stimulation of its ipsilateral receptive field. Note that the ipsilateral input can be affected even in the neuron that does not receive contralateral supply. This can reduce the noxious threshold for the ipsilateral receptive field and increase the nociceptive afferent discharge reaching the PN, thereby contributing to development of allodynia and hyperalgesia on the uninjured side (Contralateral Hypersensitivity). The hyperalgesia can further be augmented by disinhibition of pathways 1 and 2 that will open a gate allowing injured afferent barrage to reach the contralateral PN. Inhibitory interneurons are shown in green, an excitatory neuron in orange.

as arising from its ipsilateral receptive field, even in the absence of activity in the afferents innervating this field. Thus, disinhibition that was shown to cause hypersensitivity and enlarge receptive fields of dorsal horn neurons (Markus and Pomeranz, 1987; Hylden et al., 1989; Yaksh, 1989; Drew et al., 2004; Torsney and MacDermott, 2006; Zeilhofer and Zeilhofer, 2008; Kim et al., 2012) can also play a crucial role in induction of mirror-image pain. Our observation that the contralateral input to Lamina I neurons is substantially smaller than their ipsilateral input can also explain the fact that the pain on the uninjured side is usually less severe than that on the side of injury (Konopka et al., 2012).

Besides, loss of the contralateral A$\beta\delta$-fiber-mediated presynaptic inhibition of the ipsilateral C-fibers can increase the afferent drive reaching Lamina I neurons on uninjured side after stimulation of their ipsilateral receptive field (pathway 3). As our data show, the ipsilateral input can be affected even in the neurons that do not receive contralateral afferent supply. This can reduce the noxious threshold for the ipsilateral receptive field and increase the nociceptive afferent discharge reaching Lamina I neurons, thereby contributing to the spread of allodynia and hyperalgesia to the uninjured side. Furthermore, the hyperalgesia can be augmented by disinhibition of pathways 1 and 2 that will allow injured afferent barrage reaching contralateral Lamina I.

In conclusion, decussating primary afferent system supplies lumbar Lamina I PNs and LCNs being subject to different forms of inhibitory control. Pathologic disinhibition of the commissural pathways or central sensitization caused by functional plasticity at synapses of primary afferents (Ikeda et al., 2003) or dorsal horn interneurons (Santos et al., 2009) can induce contralateral allodynia, hyperalgesia and mirror-image pain.

References

Al Ghamdi KS, Polgár E, Todd AJ (2009) Soma size distinguishes projection neurons from neurokinin 1 receptor-expressing interneurons in lamina I of the rat lumbar spinal dorsal horn. Neuroscience 164:1794–1804.

Antal Z, Luz LL, Safronov BV, Antal M, Szücs P (2016) Neurons in the lateral part of the lumbar spinal cord show distinct novel axon trajectories and are excited by short propriospinal ascending inputs. Brain Struct Funct 221:2343–2360.

Barron DH, Matthews BH (1938) The interpretation of potential changes in the spinal cord. J Physiol 92:276–321.

Brown AG (1982) The dorsal horn of the spinal cord. Q J Exp Physiol 67:193–212.

Brown AG, Kirk EJ, Martin HF 3rd (1973) Descending and segmental inhibition of transmission through the spinocervical tract. J Physiol 230:689–705.

Burstein R, Dado RJ, Giesler GJ Jr (1990) The cells of origin of the spinothalamic tract of the rat: a quantitative reexamination. Brain Res 511:329–337.

Cheng CF, Cheng JK, Chen CY, Lien CC, Chu D, Wang SY, Tsaur ML (2014) Mirror-image pain is mediated by nerve growth factor produced from tumor necrosis factor alpha-activated satellite glia after peripheral nerve injury. Pain 155:906–920.

Coderre TJ, Melzack R (1991) Central neural mediators of secondary hyperalgesia following heat injury in rats: neuropeptides and excitatory amino acids. Neurosci Lett 131:71–74.

Coderre TJ, Katz J, Vaccarino AL, Melzack R (1993) Contribution of central neuroplasticity to pathological pain: review of clinical and experimental evidence. Pain 52:259–285.

Culberson JL, Haines DE, Kimmel DL, Brown PB (1979) Contralateral projection of primary afferent fibers to mammalian spinal cord. Exp Neurol 64:83–97.

Drew GM, Siddall PJ, Duggan AW (2004) Mechanical allodynia following contusion injury of the rat spinal cord is associated with loss of GABAergic inhibition in the dorsal horn. Pain 109:379–388.

Fernandes EC, Luz LL, Mytakhir O, Lukoyanov NV, Szucs P, Safronov BV (2016) Diverse firing properties and Aβ-, Aδ-, and C-afferent inputs of small local circuit neurons in spinal lamina I. Pain 157:475–487.

Fernandes EC, Santos IC, Kokai E, Luz LL, Szucs P, Safronov BV (2018) Low- and high-threshold primary afferent inputs to spinal lamina III antenna-type neurons. Pain 159:2214–2222.

Fernandes EC, Pechincha C, Luz LL, Kokai E, Szucs P, Safronov BV (2020) Primary afferent-driven presynaptic inhibition of C-fiber inputs to spinal lamina I neurons. Prog Neurobiol 188:101786.

Fernandes EC, Carlos-Ferreira J, Luz LL, Safronov BV (2022a) Presynaptic interactions between trigeminal and cervical nociceptive afferents supplying upper cervical lamina I neurons. J Neurosci 42:3587–3598.

Fernandes EC, Carlos-Ferreira J, Luz LL, Kokai E, Meszar Z, Szucs P, Safronov BV (2022b) Processing of trigeminocervical nociceptive afferent input by neuronal circuity in the upper cervical lamina I. Pain 163:362–375.

Fitzgerald M (1982) The contralateral input to the dorsal horn of the spinal cord in the decerebrate spinal rat. Brain Res 236:275–287.

Fitzgerald M (1983) Influences of contralateral nerve and skin stimulation on neurones in the substantia gelatinosa of the rat spinal cord. Neurosci Lett 36:139–143.

Huang D, Yu B (2010) The mirror-image pain: an unclered phenomenon and its possible mechanism. Neurosci Biobehav Rev 34:528–532.

Hylden JLK, Nahin RL, Traub RJ, Dubner R (1989) Expansion of receptive fields of spinal lamina I projection neurons in rats with unilateral adjuvant-induced inflammation: the contribution of dorsal horn mechanisms. Pain 37:229–243.

Ibuki T, Hama AT, Wang XT, Pappas GD, Sagen J (1997) Loss of GABA-immunoreactivity in the spinal dorsal horn of rats with peripheral nerve injury and promotion of recovery by adrenal medullary grafts. Neuroscience 76:845–858.

Ikeda H, Heinke B, Ruscheweyh R, Sandkühler J (2003) Synaptic plasticity in spinal lamina I projection neurons that mediate hyperalgesia. Science 299:1237–1240.

Khan AA, Owatz CB, Schindler WG, Schwartz SA, Keiser K, Hargreaves KM (2007) Measurement of mechanical allodynia and local anesthetic efficacy in patients with irreversible pulpitis and acute periradicular periodontitis. J Endod 33:796–799.

Kim YH, Back SK, Davies AJ, Jeong H, Jo HJ, Chung G, Na HS, Bae YC, Kim SJ, Kim JS, Jung SJ, Oh SB (2012) TRPV1 in GABAergic interneurons mediates neuropathic mechanical allodynia and disinhibition of the nociceptive circuitry in the spinal cord. Neuron 74:640–647.

Kokai E, Luz LL, Fernandes EC, Safronov BV, Poisbeau P, Szucs P (2022) Quantitative spatial analysis reveals that the local axons of lamina I projection neurons and interneurons exhibit distributions that predict distinct roles in spinal sensory processing. J Comp Neurol 530:3270–3287.

Koltzenburg M, Wall PD, McMahon SB (1999) Does the right side know what the left is doing? Trends Neurosci 22:122–127.

Konopka KH, Harbers M, Houghton A, Kortekaas R, van Vliet A, Timmerman W, den Boer JA, Struys MM, van Wijhe M (2012) Bilateral sensory abnormalities in patients with unilateral neuropathic pain; a quantitative sensory testing (QST) study. PLoS One 7:e37524.

Krotov V, Tokhtamysh A, Safronov BV, Belan P, Voitenko N (2019) High-threshold primary afferent supply of spinal lamina X neurons. Pain 160:1982–1988.

Krotov V, Agashkov K, Krasniakova M, Safronov BV, Belan P, Voitenko N (2022) Segmental and descending control of primary afferent input to the spinal lamina X. Pain 163:2014–2020.

Li J, Baccei ML (2011) Pacemaker neurons within newborn spinal pain circuits. J Neurosci 31:9010–9022.

Light AR, Perl ER (1979a) Reexamination of the dorsal root projection to the spinal dorsal horn including observations on the differential termination of coarse and fine fibers. J Comp Neurol 186:117–131.

Light AR, Perl ER (1979b) Spinal termination of functionally identified primary afferent neurons with slowly conducting myelinated fibers. J Comp Neurol 186:133–150.

Lloyd DP, McIntyre AK (1949) On the origins of dorsal root potentials. J Gen Physiol 32:409–443.

Luz LL, Szucs P, Safronov BV (2014) Peripherally driven low-threshold inhibitory inputs to lamina I local-circuit and projection neurones: a new circuit for gating pain responses. J Physiol 592:1519–1534.

Luz LL, Fernandes EC, Dora F, Lukoyanov NV, Szucs P, Safronov BV (2019) Trigeminal Aδ- and C-afferent supply of lamina I neurons in the trigeminocervical complex. Pain 160:2612–2623.

Marfurt CF, Rajchert DM (1991) Trigeminal primary afferent projections to "non-trigeminal" areas of the rat central nervous system. J Comp Neurol 303:489–511.

Markus H, Pomeranz B (1987) Saphenous has weak ineffective synapses in sciatic territory of rat spinal cord: electrical stimulation of the saphenous or application of drugs reveal these somatotopically inappropriate synapses. Brain Res 416:315–321.

Mathew NT, Kailasam J, Meadors L (2008) Predictors of response to botulinum toxin type A (BoNTA) in chronic daily headache. Headache 48:194–200.

Mendell LM (1966) Physiological properties of unmyelinated fiber projection to the spinal cord. Exp Neurol 16:316–332.

Milligan ED, Twining C, Chacur M, Biedenkapp J, O'Connor K, Poole S, Tracey K, Martin D, Maier SF, Watkins LR (2003) Spinal glia and proinflammatory cytokines mediate mirror-image neuropathic pain in rats. J Neurosci 23:1026–1040.

Petkó M, Antal M (2000) Propriospinal afferent and efferent connections of the lateral and medial areas of the dorsal horn (laminae I-IV) in the rat lumbar spinal cord. J Comp Neurol 422:312–325.

Petkó M, Veress G, Vereb G, Storm-Mathisen J, Antal M (2004) Commissural propriospinal connections between the lateral aspects of laminae III-IV in the lumbar spinal cord of rats. J Comp Neurol 480:364–377.

Pfaller K, Arvidsson J (1988) Central distribution of trigeminal and upper cervical primary afferents in the rat studied by anterograde transport of horseradish peroxidase conjugated to wheat germ agglutinin. J Comp Neurol 268:91–108.

Pinto V, Szücs P, Derkach VA, Safronov BV (2008) Monosynaptic convergence of C- and Adelta-afferent fibres from different segmental dorsal roots on to single substantia gelatinosa neurones in the rat spinal cord. J Physiol 586:4165–4177.

Pinto V, Szucs P, Lima D, Safronov BV (2010) Multisegmental Aδ- and C-fiber input to neurons in lamina I and the lateral spinal nucleus. J Neurosci 30:2384–2395.

Réthelyi M, Trevino DL, Perl ER (1979) Distribution of primary afferent fibers within the sacrococcygeal dorsal horn: an autoradiographic study. J Comp Neurol 185:603–621.

Rudomin P, Schmidt RF (1999) Presynaptic inhibition in the vertebrate spinal cord revisited. Exp Brain Res 129:1–37.

Safronov BV, Pinto V, Derkach VA (2007) High-resolution single-cell imaging for functional studies in the whole brain and spinal cord and thick tissue blocks using light-emitting diode illumination. J Neurosci Methods 164:292–298.

Santos SF, Luz LL, Szucs P, Lima D, Derkach VA, Safronov BV (2009) Transmission efficacy and plasticity in glutamatergic synapses formed by excitatory interneurons of the substantia gelatinosa in the rat spinal cord. PLoS One 4:e8047.

Schindelin J, Arganda-Carreras I, Frise E, Kaynig V, Longair M, Pietzsch T, Preibisch S, Rueden C, Saalfeld S, Schmid B, Tinevez JY, White DJ, Hartenstein V, Eliceiri K, Tomancak P, Cardona A (2012) Fiji: an open-source platform for biological-image analysis. Nat Methods 9:676–682.

Shehab SA, Hughes DI (2011) Simultaneous identification of unmyelinated and myelinated primary somatic afferents by co-injection of isolectin B4 and Cholera toxin subunit B into the sciatic nerve of the rat. J Neurosci Methods 198:213–221.

Simpson RK Jr, Huang W (1998) Glycine receptor reduction within segmental gray matter in a rat model in neuropathic pain. Neurol Res 20:161–168.

Sotgiu ML, Brambilla M, Valente M, Biella GE (2004) Contralateral input modulates the excitability of dorsal horn neurons involved in noxious signal processes. Potential role in neuronal sensitization. Somatosens Mot Res 21:211–215.

Spike RC, Puskár Z, Andrew D, Todd AJ (2003) A quantitative and morphological study of projection neurons in lamina I of the rat lumbar spinal cord. Eur J Neurosci 18:2433–2448.

Su YS, Mei HR, Wang CH, Sun WH (2018) Peripheral 5-HT3 mediates mirror-image pain by a cross-talk with acid-sensing ion channel 3. Neuropharmacology 130:92–104.

Swett JE, Torigoe Y, Elie VR, Bourassa CM, Miller PG (1991) Sensory neurons of the rat sciatic nerve. Exp Neurol 114:82–103.

Szucs P, Pinto V, Safronov BV (2009) Advanced technique of infrared LED imaging of unstained cells and intracellular structures in isolated spinal cord, brainstem, ganglia and cerebellum. J Neurosci Methods 177:369–380.

Szucs P, Luz LL, Lima D, Safronov BV (2010) Local axon collaterals of lamina I projection neurons in the spinal cord of young rats. J Comp Neurol 518:2645–2665.

Szucs P, Luz LL, Pinho R, Aguiar P, Antal Z, Tiong SY, Todd AJ, Safronov BV (2013) Axon diversity of lamina I local-circuit neurons in the lumbar spinal cord. J Comp Neurol 521:2719–2741.

Takahashi Y, Chiba T, Sameda H, Ohtori S, Kurokawa M, Moriya H (2002) Organization of cutaneous ventrodorsal and rostrocaudal axial lines in the rat hindlimb and trunk in the dorsal horn of the spinal cord. J Comp Neurol 445:133–144.

Takahashi Y, Chiba T, Kurokawa M, Aoki Y (2003) Dermatomes and the central organization of dermatomes and body surface regions in the spinal cord dorsal horn in rats. J Comp Neurol 462:29–41.

Torsney C, MacDermott AB (2006) Disinhibition opens the gate to pathological pain signaling in superficial neurokinin 1 receptor-expressing neurons in rat spinal cord. J Neurosci 26:1833–1843.

Wall PD, Lidierth M (1997) Five sources of a dorsal root potential: their interactions and origins in the superficial dorsal horn. J Neurophysiol 78:860–871.

Warwick C, Salsovic J, Hachisuka J, Smith KM, Sheahan TD, Chen H, Ibinson J, Koerber HR, Ross SE (2022) Cell type-specific calcium imaging of central sensitization in mouse dorsal horn. Nat Commun 13:5199.

Willis WD Jr (1999) Dorsal root potentials and dorsal root reflexes: a double-edged sword. Exp Brain Res 124:395–421.

Woolf CJ, Fitzgerald M (1986) Somatotopic organization of cutaneous afferent terminals and dorsal horn neuronal receptive fields in the superficial and deep laminae of the rat lumbar spinal cord. J Comp Neurol 251:517–531.

Yaksh TL (1989) Behavioral and autonomic correlates of the tactile evoked allodynia produced by spinal glycine inhibition: effects of modulatory receptor systems and excitatory amino acid antagonists. Pain 37:111–123.

Zeilhofer HU, Zeilhofer UB (2008) Spinal dis-inhibition in inflammatory pain. Neurosci Lett 437:170–174.